DEVELOPMENTAL DYNAMICS 235:3144–3155, 2006

The RNA Binding Protein *Zfp36l1* Is Required for Normal Vascularisation and Post-Transcriptionally Regulates VEGF Expression°

Sarah E. Bell,[1]* Maria Jose Sanchez,[2†] Olivera Spasic-Boskovic,[3] Tomas Santalucia,[4‡] Laure Gambardella,[1] Graham J. Burton,[3] John J. Murphy,[5] John D. Norton,[6] Andrew R. Clark,[4] and Martin Turner[1]

The *Zfp36l1* gene encodes a zinc finger-containing mRNA binding protein implicated in the posttranscriptional control of gene expression. Mouse embryos homozygous for a targeted mutation in the *Zfp36l1* locus died mid-gestation and exhibited extraembryonic and intraembryonic vascular abnormalities and heart defects. In the developing placenta, there was a failure of the extraembryonic mesoderm to invaginate the trophoblast layer. The phenotype was associated with an elevated expression of vascular endothelial growth factor (VEGF)-A in the embryos and in embryonic fibroblasts cultured under conditions of both normoxia and hypoxia. VEGF-A overproduction by embryonic fibroblasts was not a consequence of changes in *Vegf-a* mRNA stability; instead, we observed enhanced association with polyribosomes, suggesting *Zfp36l1* influences translational regulation. These data implicate *Zfp36l1* as a negative regulator of *Vegf-a* gene activity during development. *Developmental Dynamics 235:3144–3155, 2006.*

Key words: Zfp36l1; VEGF; extraembryonic and intraembryonic vasculature

Accepted 4 August 2006

INTRODUCTION

Zfp36l1 (also called TIS11b, BRF-1, Berg36, cMG1, ERF-1) (Gomperts et al., 1990; Varnum et al., 1991; Barnard et al., 1993; Bustin et al., 1994; Maclean et al., 1995; Ning et al., 1996) belongs to a family of mRNA-binding proteins possessing an unusual and highly conserved zinc finger motif, comprising a tandem YKTEL $CX_8CX_5CX_3H$ sequence, spaced exactly 18 amino acids apart. The prototype of this family, tristetraprolin (TTP, Tis11, Nup475, G0S24) (Varnum et al., 1989; DuBois et al., 1990; Lai et al., 1990; Ma and Herschman, 1991; Heximer and Forsdyke, 1993) is the product of an immediate early response gene *Zfp36* in the mouse.

°This article was accepted for inclusion in *Developmental Dynamics* 235 #9–Mouse Development Special Issue.
The Supplementary Material referred to in this article can be viewed at www.interscience.wiley.com/jpages/1058-8388/suppmat
[1]Laboratory of Lymphocyte Signalling and Development, The Babraham Institute, Babraham Research Campus, Babraham, Cambridge, United Kingdom
[2]Department of Haematology, University of Cambridge, Cambridge Institute for Medical Research, Cambridge, United Kingdom
[3]Department of Anatomy, University of Cambridge, Cambridge, United Kingdom
[4]The Kennedy Institute of Rheumatology, Imperial College London, London, United Kingdom
[5]Infection and Immunity Research Group, Kings College London, University of London, London, United Kingdom
[6]Department of Biological Sciences, University of Essex, Colchester, United Kingdom
Grant sponsor: Leukaemia Research Fund; Grant sponsor: Association for International Cancer Research; Grant sponsor: Biotechnology and Biological Sciences Research Council; Grant sponsor: MRC; Grant sponsor: Ministerio de Educacion y Ciencia; Grant number: SAF2003-07214.
†Maria Jose Sanchez's present address is Centro Andaluz de Biologia de Desarrollo (CSIC UPO), Universidad Pablo de Olavide, Carretera de Utrera Km 1, 41013 Sevilla, Spain
‡Tomas Santalucia's present address is Institut d'Investigacions Biomediques de Barcelona (CSIC/IDIBAPS), Rossello 161, 08036 Barcelona, Spain
***Correspondence to: Sarah E. Bell, Laboratory of Lymphocyte Signalling and Development, The Babraham Institute, Babraham Research Campus, Cambridge, CB2 4AT, UK. E-mail: sarah-e.bell@bbsrc.ac.uk**

DOI 10.1002/dvdy.20949
Published online 29 September 2006 in Wiley InterScience (www.interscience.wiley.com).

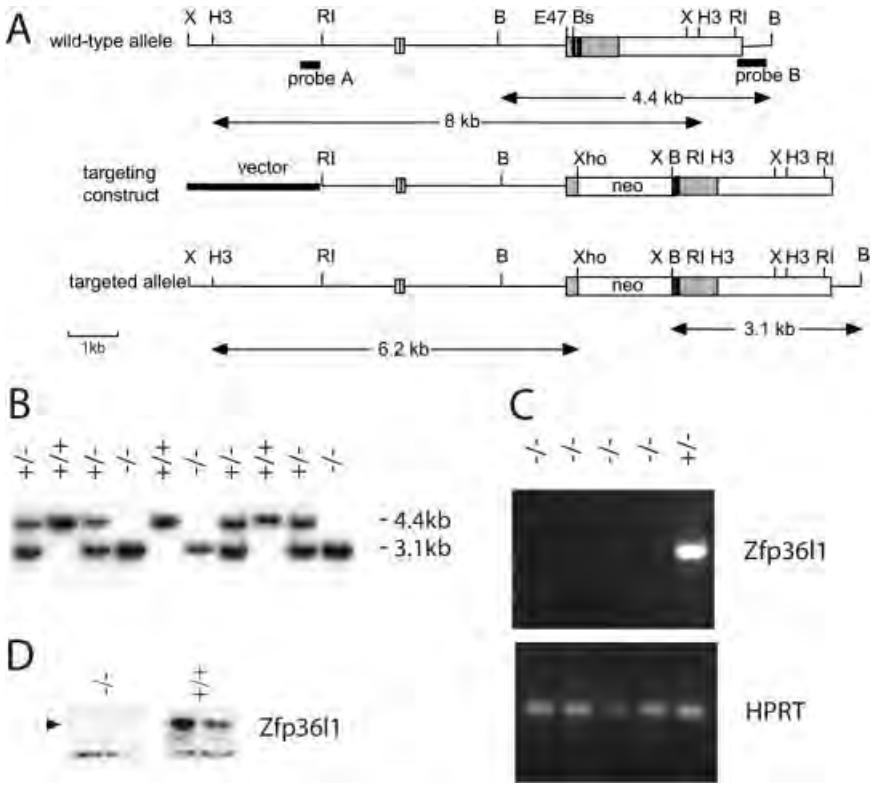

Fig. 1. Targeted disruption of the mouse *Zfp36l1* gene. **A:** Targeting scheme. The top panel shows the genomic organization of the *Zfp36l1* gene. The two exons are indicated by the boxed areas; the coding region is contained within the shaded area; the 5′ and 3′ UTR within the unshaded area; the positions of the two zinc fingers are indicated by black boxes. The middle panel represents the targeting vector. The bottom panel represents the predicted structure of the *Zfp36l1* locus following homologous recombination. The external probes used for Southern analysis and predicted sizes of fragments are indicated. Restriction sites are indicated B, *Bam*HI; Bs, *Bst*BI; E47, *Eco*47III; H3, *Hin*dIII; RI, *Eco*RI; X, *Xba*I; Xho, *Xho*I. **B:** Genotyping of E9.5 embryo DNA from heterozygous matings. DNA was digested with *Bam*HI, and analysed with probe B. Wild-type (4.4 kb) and mutant (3.1 kb) bands are indicated. **C:** RT PCR analysis of total RNA from *Zfp36l1* heterozygous (+/−) and homozygous (−/ −) E9.5 embryos. PCR analysis of *Zfp36l1* mRNA in embryos is shown in the top panel; analysis of *Hprt* mRNA is shown in the bottom panel. **D:** Western blot analysis of cell lysates from *Zfp36l1* homozygous (−/ −) and wild-type (+/+) MEF. The position of the Zfp36l1 protein is indicated by an arrow. The lower band is non-specific.

TTP and its mammalian relatives, Zfp36l1, Zfp36l2, and Zfp36l3, have been shown to play a role in regulating mRNA stability by virtue of their binding to AU-rich elements (AREs) common to the 3′ untranslated region (3′ UTR) of acutely regulated genes. Binding promotes deadenylation and degradation of target mRNA leading to lowered gene activity (Lai et al., 2000). Mutation of *Zfp36l1* in the mouse has been reported to give rise to chorioallantoic fusion defects through unknown mechanisms (Stumpo et al., 2004); mutation of *Zfp36l2* causes female infertility (Ramos et al., 2004); and *Zfp36*-deficient mice exhibit a rapidly developing autoimmune syndrome that is attributable to overproduction of TNFα (Taylor et al., 1996; Carballo et al., 1997). To understand the function of *Zfp36l1*, we generated mice in which the *Zfp36l1* gene was inactivated by homologous recombination. We show here that Zfp36l1-mutant embryos exhibit extraembryonic and intraembryonic vascular defects, neural tube defects, and cardiac abnormalities. We also identify *Vegf-a* as a gene whose expression is elevated by loss of Zfp36l1 and show evidence for Zfp36l1 in the regulation of translation.

RESULTS

Zfp36l1 Mutant Embryos Exhibited Vascular Abnormalities

The integrity of the zinc finger domains of TTP, Zfp36l1, and Zfp36l2 has been shown to be essential for binding to AREs and for the promotion of target mRNA degradation (Lai et al., 1999). Consequently, disruption of this region of Zfp36l1 should ablate any functional activity. Therefore, a null allele of *Zfp36l1* was produced by replacement of part of the amino terminus and first zinc finger contained within exon 2 with a neomycin cassette that also disrupted the reading frame (Fig. 1A). Germline transmission of the targeted disruption of the *Zfp36l1* locus was obtained from two independently targeted ES cell clones. Heterozygous *Zfp36l1*$^{+/-}$ mice from both lines appeared normal and were intercrossed to generate mice homozygous for the targeted mutation. In over 300 pups born from both lines, no homozygous mutant (*Zfp36l1*$^{-/-}$) offspring were identified indicating that the null mutation was lethal (data not shown). Viable *Zfp36l1*$^{-/-}$ embryos with beating hearts were identified at E9.5, but by E10.5 all mutant embryos had died showing severe growth retardation and/or developmental defects. Heterozygous embryos could not be distinguished morphologically from wild-type embryos at E9.5 or E10.5. Generation of homozygous mutant *Zfp36l1*$^{-/-}$ embryos at E9.5 was demonstrated by Southern blot analysis of visceral yolk sac DNA (Fig. 1B). RT-PCR analysis using RNA obtained from E9.5 embryos was performed using intron-spanning primers and identified a product of the predicted size in cDNA from wild-type and heterozygous embryos but yielded no product in cDNA from mutant embryos (Fig. 1C). Furthermore, Western blot analysis confirmed the absence of Zfp36l1 protein in mouse embryonic fibroblasts (MEF) derived from mutant embryos (Fig. 1D). Together, these results demonstrate that we have generated a null allele that results in embryonic lethality.

Analysis of *Zfp36l* expression in normal embryos at E8.5 using in situ hybridisation revealed *Zfp36l1* mRNA was diffusely expressed throughout the embryo with highest expression seen in the chorion and blood vessels of the maternal decidua (Fig. 2A). At E9.5, the highest levels of expression were seen in the neural tube, paraxial mesoderm, brain, and otic vesicle (Fig. 2B, left panel). Furthermore, *Zfp36l1* mRNA was detected in the yolk sac at

this stage by RT-PCR (data not shown). This expression pattern correlated with defects visible in the yolk sac and in whole mount of *Zfp36l1*-deficient embryos. When the visceral yolk sac of E9.5 mutant embryos was compared to that of wild-type embryos, it appeared paler, contained areas of hemorrhage, and exhibited reduced branching of the vitelline vessels, suggestive of a defect in vascular organization. As a tool to examine blood vessel formation, *Zfp36l1*$^{+/-}$ animals were interbred with transgenic mice expressing a *lacZ* reporter under the control of the *SCL* promoter and 3′ enhancer (Sanchez et al., 1999). These mice exhibit *lacZ* expression specifically in blood vessels and hematopoietic tissue. X-gal staining of embryos in whole-mount revealed that in the yolk sac of the mutant embryos, there was a lack of an organised yolk sac vasculature and that the capillary network appeared less well structured (Fig. 3A, left panel). Examination at a higher magnification revealed that vitelline vessels were present but failed to undergo extensive branching in the mutant yolk sac (Fig. 3B) and that an organised vascular cell network was absent. The yolk sac vessels also appeared narrower in the mutant compared to the control (Fig. 3B). Histological analysis revealed that the structure of the visceral yolk sac and blood islands was grossly normal in *Zfp36l1*-deficient embryos and suggested that there was a reduction in the total number of blood cells within the blood islands (Fig. 4A, left panel). The mean number of cells recovered per yolk sac was $18.8 \pm 3.9 \times 10^4$ from control embryos compared with $3.8 \pm 1.7 \times 10^4$ cells from *Zfp36l1*-deficient embryos (Table 1). Cells isolated from the yolk sac were analysed by flow cytometry using antibodies against TER119 (a marker of erythroid cells) and c-kit (a marker of hematopoietic progenitors). As shown in Figure 4B and Table 1, the proportion and absolute number of TER119$^+$ cells was dramatically reduced in the yolk sac from *Zfp36l1*-deficient embryos, whereas the absolute number of c-kit$^+$ cells was similar to that in control embryos (Table 1). These data demonstrate that the reduction in the number of cells present in the mutant yolk sac largely reflected a loss of committed TER119$^+$ erythroid cells, whereas the number of progenitors appeared normal. This would account for the pale appearance of the yolk sac in the mutant embryos. Thus, *Zfp36l1* is required for extraembryonic vasculogenesis and expansion of primitive erythroid cells in the yolk sac. In whole mount E9.5 mutant embryos also appeared anemic compared to littermate controls. In agreement with the reduction in TER119$^+$ cells observed in the yolk sac, histological analysis revealed that there was a reduction in the number of circulating blood cells in *Zfp36l1*$^{-/-}$ embryos compared to controls (Fig. 4C, left panel, arrowed).

The high level of expression of *Zfp36l1* mRNA seen by in situ hybridisation in the neural tube and paraxial mesoderm correlated with defects visible in whole-mount mutant embryos including undulations in the

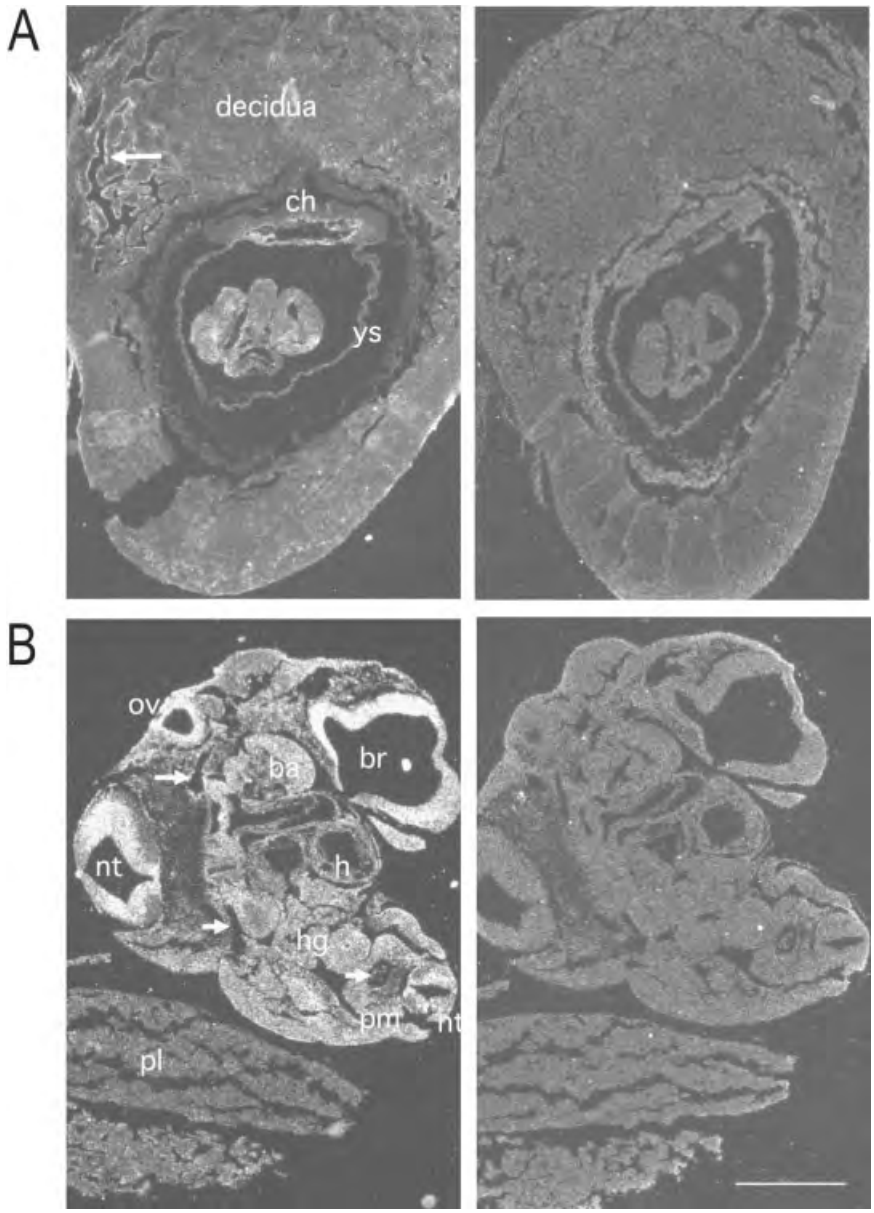

Fig. 2. Expression of *Zfp36l1* mRNA at E8.5 and E9.5. In situ hybridisation with anti-sense (left) and sense (right) probes. **A**, left panel: The position of the chorion is indicated (ch); blood vessels of the maternal decidua are arrowed; yolk sac (ys). **B**, left panel: E9.5 embryo in sagittal section. br, brain; ov, otic vesicle; nt, neural tube; pm, paraxial mesoderm; hg, endoderm of the hindgut; ba, branchial arch; h, heart; pl, placenta. The aorta is arrowed. Original magnification ×25. Scale bar = 1 mm.

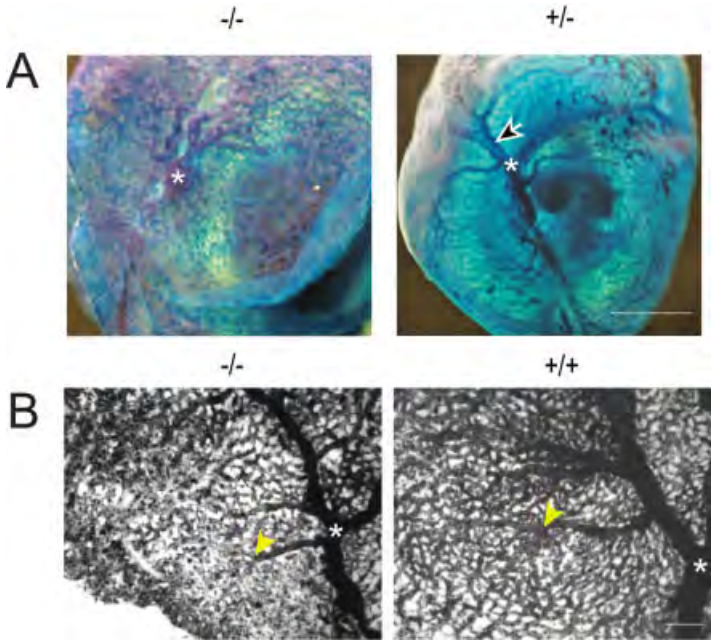

Fig. 3.

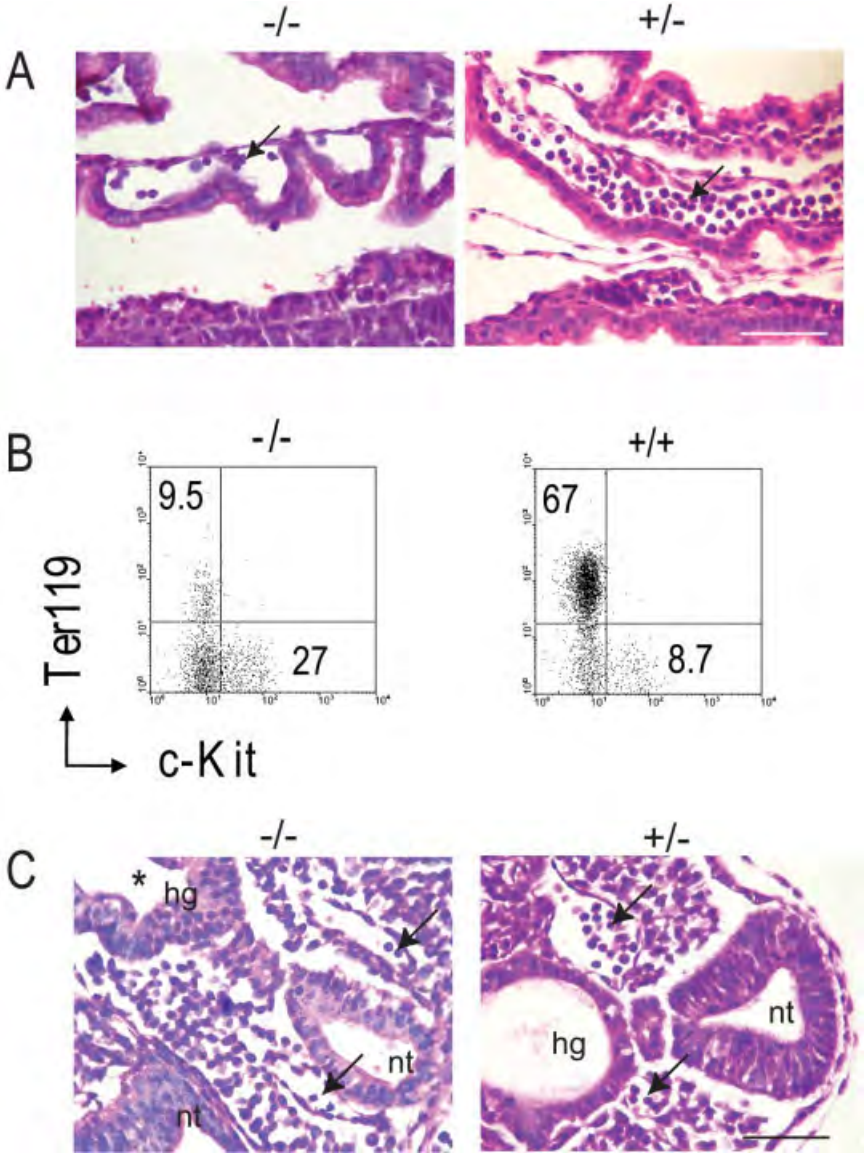

Fig. 4.

neural tube at or below the forelimb bud, irregularities in somite organization, and abnormal flexure of the tail (Figs. 4C, 5A, left panels). PECAM staining of whole-mount embryos indicated that intersomitic vessels were formed in mutant embryos but often did not extend fully dorso-ventrally along the somites (Fig. 5A, left panel). X-gal staining of *SCL lacZ* transgenic embryos was used to further visualise embryonic vessels in whole-mount. Embryos were examined by light microscopy and by optical projection tomography (Sharpe et al., 2002). Defects in intraembryonic vasculature were observed in *Zfp36l1*-deficient embryos (Fig. 5B,C left panels; see Supplemental Movie S1, which can be viewed at www.interscience.wiley.com/jpages/1058-8388/suppmat); the dorsal aorta was enlarged and appeared disorganised both cranially and caudally. The organisation and expansion of the intersomitic vessels was abnormal in mutant embryos. There was also a failure of vessels to

Fig. 3. Analysis of the yolk sac vasculature at E9.5. **A:** Whole mount view of a *Zfp36l1*$^{-/-}$ (left) and control *Zfp36l1*$^{+/-}$ embryo (right). *SCL lacZ* transgenic embryos were stained with X-gal. Pictures show the yolk sac surrounding the embryo. Original magnification ×30. Note the absence of an organised yolk sac vasculature in the mutant embryo (arrowed in wild-type). A branch in the major vitelline vessel is indicated by an asterisk. Scale bar = 1 mm. **B:** *Zfp36l1*$^{-/-}$ (left) and control *Zfp36l1*$^{+/+}$ yolk sacs (right) were mounted under coverslips and viewed under phase contrast. Extensive branching of the yolk sac vessels was seen in the wild-type (yellow arrowhead), but absent in the mutant embryo. The asterisk represents the branch point illustrated in A. A different control yolk sac is shown in A and B, for better comparison to the mutant. Original magnification ×100. Scale bar = 0.2 mm.

Fig. 4. Analysis of blood cells at E9.5. **A:** Hematoxylin and eosin stained sections demonstrating yolk sac blood islands. Blood cells within the blood islands are arrowed. Original magnification ×200. Scale bar = 0.1 mm. **B:** Flow cytometric analysis of yolk sac tissue. Cell suspensions prepared from individual E9.5 yolk sacs were stained with antibodies against TER119 and c-kit. Percentage values are shown in each quadrant. **C:** Histological analysis of intraembryonic circulation at E9.5. H & E stained transverse sections from mutant (−/−), and control (+/−) embryos. In the para-aortic splanchnopleura region, the paired vessels of the dorsal aorta are arrowed; neural tube (nt) and hindgut (hg). Original magnification ×200. Dorsal aspect to the right. *, an irregularity in the hindgut. Scale bar = 0.1 mm.

TABLE 1. Flow Cytometric Analysis of Yolk Sac Tissue From E9.5 Embryos[a]

Embryo genotype	Total number of cells per yolk sac[b]	Number of TER119$^+$ cells	Number of c-kit$^+$ cells
Zfp36/1−/− (n = 8)	3.8 ± 1.7	1.4 ± 1.1	2.1 ± 1.3
Zfp36/1+/− (n = 5)	18.8 ± 3.9	13.6 ± 2.0	2.3 ± 0.5

[a]Values are mean ± SEM.
[b]Cell number ($\times 10^4$).

extend fully dorso-ventrally along the somites, compared to control embryos (Fig. 5B,C; see Supplemental Movie S2). In the head, the cranial vessels failed to expand into the vascular network seen in the control. The mutant embryos also appeared slightly growth retarded. Histological analysis revealed that some intraembryonic circulation was present in the mutant embryos; in the para-aortic splanchnopleura region, the paired vessels of the dorsal aorta were observed (Fig. 4C, left panel) indicating some degree of vascular functionality.

Zfp36l1 mRNA was also expressed in the embryonic heart at day 9.5 and mutant embryos exhibited defects in the developing heart at this stage (Fig. 6). To examine cardiac structure in detail, E9.5 embryos were embedded in epoxy resin before sectioning. The trabeculae and sinusoids in the myocardial wall of the heart were less well developed and the myocardial trabecular system of the ventricles was less complex exhibiting a discontinuous endocardium (Fig. 6, left panels). Since endothelial precursor cells contribute to the formation of both the endocardium and major blood vessels during embryonic vasculogenesis, disorganisation of the endocardium is consistent with Zfp36l1 being required for normal organisation of the intraembryonic vasculature.

A previous study described a high frequency of chorioallantoic fusion defects in *Zfp36l1*$^{-/-}$ embryos (Stumpo et al., 2004). We observed that the vascular network of PECAM-1$^+$ cells in the chorion layer failed to develop normally (Fig. 7A) suggesting a defect in vasculogenesis. Immunohistochemical analysis of the developing placenta at E9–9.5 using an antibody to cytokeratin revealed that the overall development of the spongiotrophoblast, the labyrinthine trophoblast, the trophoblast giant cells, and invasion into the decidua appeared similar in control and *Zfp36l1*$^{-/-}$ embryos (Fig. 7B). However, there was a failure of the allantoic mesoderm to invaginate into the chorionic trophoblast to form the labyrinth layer of the placenta (Fig. 7B) and, consequently, this trophoblast region was abnormally compact. In mutant embryos, the interface between the chorionic/labyrinth trophoblast and the maternal blood space was almost linear and fetal capillaries containing nucleated erythrocytes were inconspicuous (Fig. 7B and D), suggesting a profound defect in angiogenesis. Immunolabelling using an antibody against von Willebrand factor produced strong staining of the maternal endothelium within the decidua and of the fetal endothelial cells of the developing labyrinth in

Fig. 5. Vascular abnormalities in E9.5 embryos. **A:** Embryos at E9.5 were stained in whole-mount with an antibody to PECAM-1. Lateral view of a mutant (−/ −) and control embryo (+/+). Original magnification ×25. Regions showing particular distortions in the neural tube are indicated by the black arrowhead. Irregular condensation of somites in the mutant is indicated by the white arrowhead (the head of each embryo was removed to determine the genotype). **B:** X-gal staining of *SCL lacZ* transgenic mutant (−/ −) and control (+/ −) embryos. The enlarged dorsal aorta is indicated by the black arrowhead and by the white arrow in the head. A region showing disorganised intersomitic vessels in the mutant is indicated by the bracket. Original magnification ×25. **C:** Optical projection tomography of X-gal stained *SCL lacZ* transgenic mutant (−/ −) and control (+/ −) embryos. al, allantois; ba, branchial artery; da, dorsal aorta; e, eye h, heart; isv, intersomitic vessels. The heart in the mutant is abnormally displaced. Scale bar = 555 μm.

Fig. 6. Cardiac defects at E9.5. **A:** In the mutant embryo the myocardial wall was thinner and less well differentiated (black arrow). The myocardial trabecular system of the ventricles is indicated by a yellow arrowhead, and the endocardium (e, small black arrowhead) was discontinuous in the mutant. Original magnification ×100. **B:** Amnion (a) in wt is absent in the mutant section. The space in the pericardium in the mutant was an artefact generated during processing, and is not seen on sections further through the embryo. Original magnification ×200. Scale bar = 0.1 mm.

Fig. 7. Defects in placental vasculogenesis. **A:** PECAM-staining of vessels in the chorion. The extensive branching of PECAM-1$^+$ vessels in the wild-type embryo (right) was absent in the mutant (arrowed, left). The embryo has been removed for photographic purposes. Original magnification ×63. **B:** Sagittal sections from the developing placenta of *Zfp36l1* mutant embryos (left) and control embryos (right) were stained with antibodies recognising cytokeratin (brown) and counterstained in blue. Invasion of the embryonic mesenchyme into the trophoblast mass was not seen in the mutant embryo, as compared to control (arrowhead). Consequently, the trophoblast mass was abnormally compact and appeared in profile as a flat sheet in the mutant and a triangular wedge in the control. Original magnification ×100. The boxed area represents a similar region on a serial section shown at higher magnification in C. **C:** Von Willebrand factor staining. Staining of fetal endothelium (arrowhead) was seen adjacent to the maternal sinuses in control, but not mutant. Note the complete absence of nucleated fetal erythrocytes from the placental vessels in the mutant, whereas these were conspicuous in the control (arrowed in control). The developing maternal blood space is indicated by an asterisk. Original magnification ×400. **D:** Hematoxylin and eosin stained sections. Serial sections to those shown in B and C. Note the complete absence of embryonic mesenchyme in the mutant (arrowhead) and of vessels containing nucleated fetal erythrocytes within the trophoblast mass (larger arrow). Maternal enucleated erythrocytes (small arrow) were seen in the blood space of the developing labyrinth in both the control and mutant. The spongiotrophoblast is indicated by an asterisk. al, Allantois; ch, chorionic trophoblast cells; lb, labyrinth layer; m, maternal decidual tissue. Original magnification ×100. Scale bar = 0.2 mm.

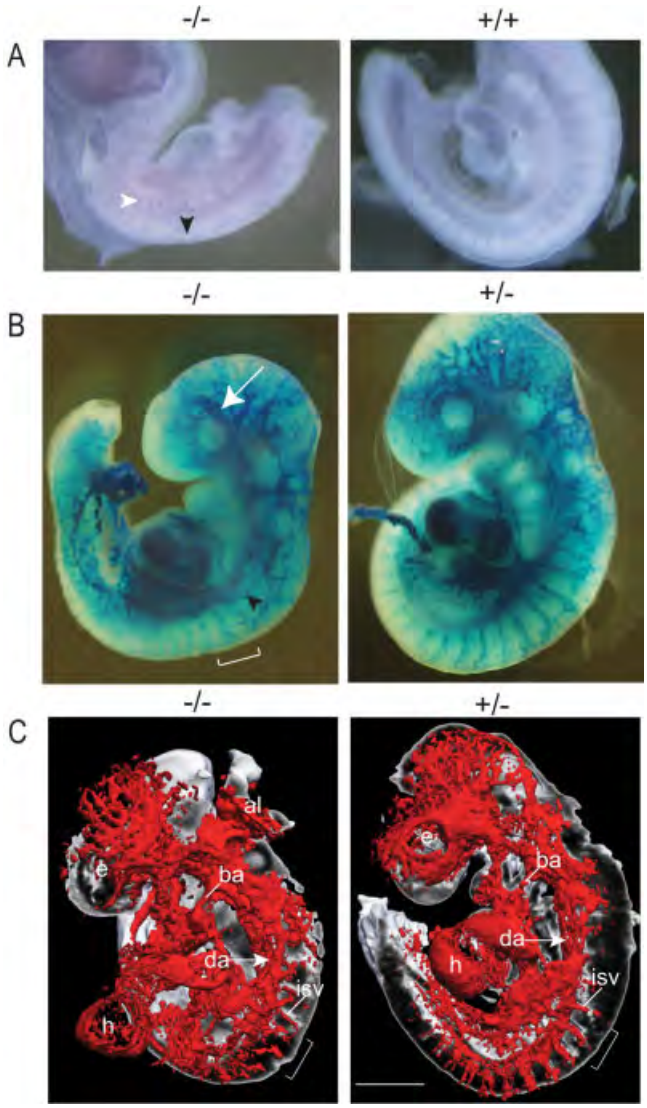

Fig. 5.

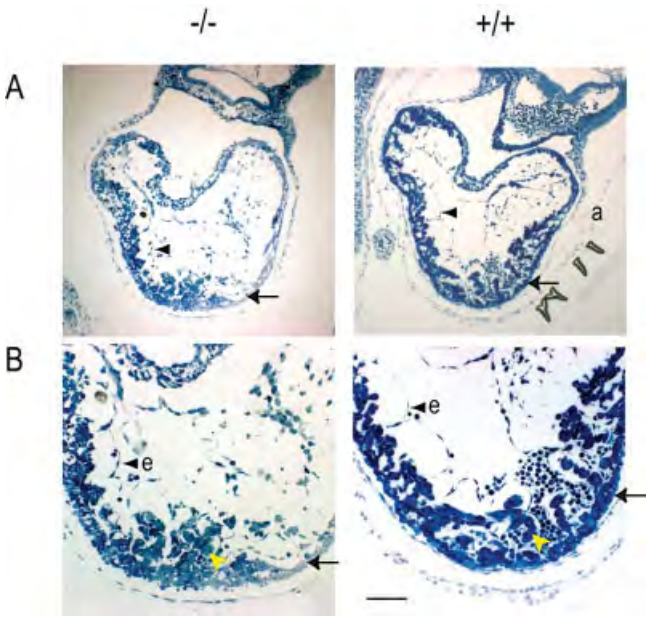

Fig. 6

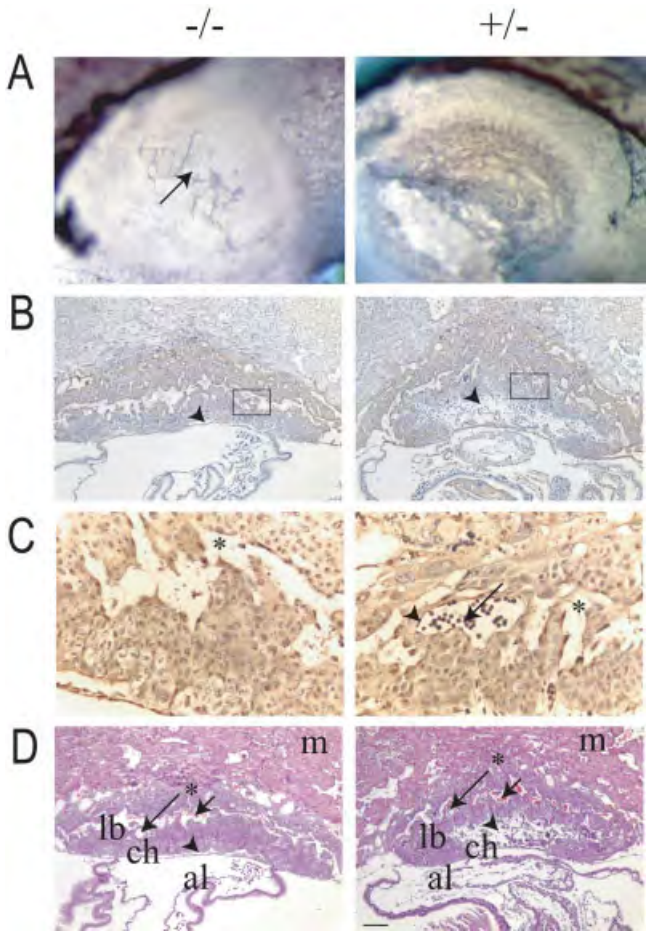

Fig. 7.

control embryos (Fig.7C, right panel). By contrast, in *Zfp36l1*$^{-/-}$ embryos, only weak staining was observed in the few vessel profiles within the labyrinth trophoblast consistent with a failure of the fetal vasculature to invaginate. Nucleated fetal erythrocytes were also absent from the placental vessel profiles in the mutant (Fig. 7C). Zfp36l1 is, therefore, required for extraembryonic vascular network formation in the yolk sac and the outgrowth of the chorioallantoic villus into the placental labyrinth. This would result in a lack of nutrient exchange between maternal and embryonic circulation and account for the growth retardation and death by E10.5. In some mouse mutants, defective vascular/heart formation may be secondary to placental abnormalities (Hemberger and Cross, 2001), and can be reversed by generating chimeras with tetraploid, wild-type cells (Barak et al., 1999; Adams et al., 2000). Unfortunately, multiple attempts to de-

rive ES cells homozygous for the *Zfp36l1*-mutation were unsuccessful precluding this line of investigation.

Zfp36l1 Post-Transcriptionally Regulates VEGF Expression

The defects observed in extraembryonic vasculogenesis in *Zfp36l1*$^{-/-}$ embryos are similar to those observed in a number of other mutant mice (Rossant and Cross, 2001), including those lacking the tumour suppressor gene *Lkb1*, which exhibited elevated VEGF-A expression (Ylikorkala et al., 2001). Since *Vegf-a* mRNA contains multiple AREs within its 3′UTR, some of which have been reported to interact with Zfp36l1 in vitro (Ciais et al., 2004), we examined VEGF-A levels in *Zfp36l1*-deficient embryos by ELISA of whole embryo extracts. VEGF-A protein was below detectable limits in wild-type embryos (<50 pg/mg embryo protein) while mutant embryos exhibited readily detectable levels of VEGF-A (85.3 ± 34.7 pg/mg embryo protein, n = 4). To examine whether elevated production of VEGF-A was only a consequence of hypoxia or glucose deprivation in the embryo, we generated embryonic fibroblasts (MEF) from mutant and wild-type embryos. We observed that VEGF-A production by cultured *Zfp36l1*$^{-/-}$ embryonic fibroblasts was elevated under both normoxic and hypoxic conditions (Fig. 8A). Elevated VEGF-A production did not correlate with increased levels of *Vegf-a* mRNA in mutant MEFs cultured under normoxic conditions; however, under hypoxic conditions the levels of *Vegf-a* mRNA was significantly elevated in *Zfp36l1*$^{-/-}$ MEF (Fig. 8B). Western blot analysis of MEF extracts with an antibody specific to glucose transporter-1 (Glut-1) showed a comparable induction of Glut-1 following hypoxia (Fig. 8C), confirming the induction of a hypoxic state. Taken together, these results demonstrate that in the absence of Zfp36l1, MEF overproduce VEGF under both normoxic and hypoxic conditions.

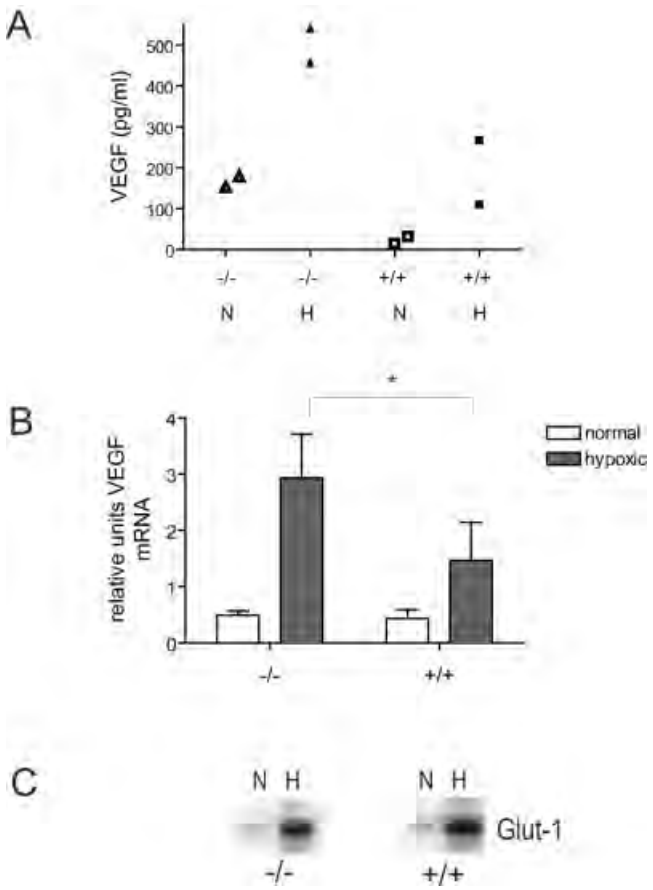

Fig. 8. Deregulated VEGF expression by *Zfp36l1*$^{-/-}$ MEF. **A:** VEGF-A levels in the supernatants of mutant (−/−, triangles) and wt (+/+, squares) fibroblasts quantified by ELISA. Values shown are from two mutant and two wt MEF lines each generated from independent littermate embryos. MEFs were incubated under normoxic (open symbols) or hypoxic conditions (filled symbols). **B:** Quantitation of *Vegf-a* mRNA in MEF cultured under normoxic or hypoxic conditions by real-time PCR. Comparative Ct values were used to calculate the quantity of *Vegf-a* RNA relative to *hprt*. Data represent the mean ± standard deviation from three independent cultures.*$P < 0.05$. **C:** Western blots of cell lysates prepared from MEF cultured under normoxic or hypoxic conditions were analysed with an antibody to Glucose transporter 1 (Glut-1).

Zfp36 family members have been shown to play a role in regulating mRNA stability following binding to AREs in the 3′ UTR of acutely regulated genes (Lai et al., 2000). To assess whether Zfp36l1 regulated *Vegf* mRNA stability, we determined the rate of *Vegf* mRNA decay following treatment of MEF with the transcriptional inhibitor actinomycin D. When tested under normoxic conditions, the rate of decay of *Vegf* mRNA was not altered in *Zfp36l1*-deficient MEF (data not shown). Furthermore, when MEF were treated with cobalt chloride (to pharmacologically mimic hypoxia) no difference was observed in mRNA decay between *Zfp36l1*-deficient and wild-type MEF (Fig. 9A), indicating that the overproduction of VEGF-A was not due to an increase in mRNA stability. We investigated the activity of the *Vegf* 3′UTR in MEF by transfection of a luciferase reporter construct containing the 3′UTR of rat *Vegf* (Ciais et al., 2004). Under normal culture conditions, or in the presence of cobalt chloride, reporter activity was higher in wild-type than in *Zfp36l1*$^{-/-}$ MEF (data not shown), suggesting that the 3′UTR of *Vegf* alone is insufficient to confer regulation by Zfp36l1. In addition to regulating RNA stability, AREs have been implicated in the translational regulation of gene expression (Zhang et al., 2002). To investigate whether *Vegf* mRNA is subject to translational regulation, we measured the distribution of *Vegf* mRNA in monosome and polysome fractions isolated from wild-type and *Zfp36l1*$^{-/-}$ MEF cultured under normoxic conditions. In comparison to wild-type MEF, *Zfp36l1*-deficient MEF exhibited enhanced *Vegf* mRNA

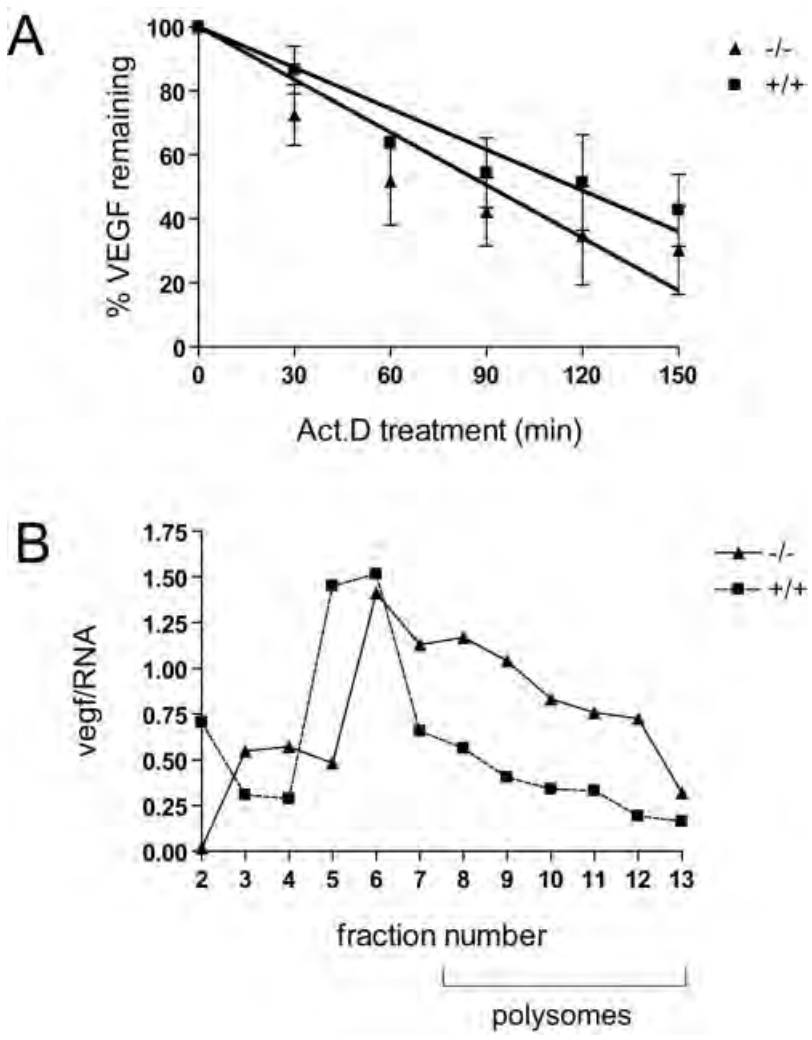

Fig. 9. Post-transcriptional regulation of *Vegf* mRNA. **A:** *Vegf* mRNA half-life in *Zfp36l1*$^{-/-}$ MEF. Data are expressed as the percentage of signal present at the onset of actinomycin D treatment. Results represent the mean ± standard deviation from three independent experiments. Half life of *Vegf* mRNA is 87 min in the mutant and 119 min in wild-type cells. **B:** Association of *Vegf* mRNA with polysomes in *Zfp36l1*$^{-/-}$ MEF. MEF were cultured under normoxic conditions. The distribution of *Vegf* mRNA in each sucrose gradient fraction is shown; the quantity of *Vegf* mRNA was determined by dot blot analysis and normalised to RNA content. These data are representative of three independent experiments. In each panel, the mutant is represented by triangles and wt by squares.

loading onto polysomes (Fig. 9B), suggesting enhanced translation of *Vegf* mRNA in the absence of Zfp36l1.

DISCUSSION

We have demonstrated a previously unappreciated role for Zfp36l1 in extraembryonic and intraembryonic vascular network formation and in the development of the heart. Furthermore, we have identified *Vegf-a* as a gene that is overexpressed in the absence of Zfp36l1. Additionally, we provide evidence that Zfp36l1 regulates VEGF at the level of translation. VEGF plays a crucial role in vasculogenesis and endocardial development (Ferrara and Davis-Smyth, 1997), which are exquisitely sensitive to increased or decreased levels of this cytokine. Notably, deletion of a single *Vegf-a* allele is sufficient to cause embryonic lethality (Carmeliet et al., 1996; Ferrara et al., 1996). Vasculogenesis also fails to occur normally in mouse embryos lacking the VEGFR-1 (Flt-1) (Fong et al., 1995). VEGF-R1 mutant embryos die around E8.5–9.0 and exhibit vascular disorganisation, while mice with a mutation of the VEGF-R1 tyrosine kinase domain develop normally (Hiratsuka et al., 1998), consistent with the idea that the main function of this receptor was the regulation of bioavailable VEGF. Indeed, recent studies show that VEGF-R1 mutant embryos exhibit defective vascular sprouting from the dorsal aorta, which can be rescued by a soluble flt-1 transgene in vitro (Kearney et al., 2004), suggesting that elevated VEGF levels disrupt correct blood vessel formation. Moreover, the administration of exogenous VEGF-A_{165} to quail embryos inhibited the formation and branching of intersomitic vessels, and led to the formation of vessels with abnormally large lumens (Drake and Little, 1995), similar to the defects observed in *Zfp36l1*-deficient embryos. Thus, elevated levels of VEGF have a profound effect on the patterning of endothelial cells involved in formation of the vascular network. A further level of regulation is mediated by the 3′UTR of *Vegf-a* mRNA (Levy et al., 1995). Uncoupling *Vegf-a* from the regulatory influences of its' 3′UTR by insertion of a *lacZ* gene gave rise to embryos with elevated VEGF-A levels, which displayed vascular and cardiac defects with similarities to those we observed in *Zfp36l1*-deficient embryos (Miquerol et al., 2000; Damert et al., 2002). Since embryonic fibroblasts lacking Zfp36l1 produced elevated levels of VEGF-A protein under both normoxic and hypoxic conditions, indicative of an intrinsic defect in the regulation of VEGF-A production, we suggest the phenotype observed in *Zfp36l1*-deficient embryos may be mediated, in part, by elevated VEGF-A. Formal proof of this notion would require a genetic rescue experiment that is not readily achievable given the lethal nature of *Vegf-a* heterozygotes. Furthermore, the failure to derive homozygous mutant *Zfp36l1* ES cells does not allow us to fully explore the nature of the phenotype through the generation of tetraploid fusions. As it has been previously noted that Zfp36l1 was expressed at high levels in ES cells (Stumpo et al., 2004), it may be that Zfp36l1 plays a crucial role in ES cells but is dispensable for the survival of fibroblasts. Overall, our data indicate that Zfp36l1 plays an important role in VEGF regulation, potentially mediated by embryonic fibroblasts in vivo, in modifying endothelial cell organisa-

tion. It is also likely that additional, currently unidentified, genes may also be over-expressed in the absence of Zfp36l1 and contribute to the phenotype. This possibility is supported by the occurrence of ARE variants in several thousand genes (Bakheet et al., 2001) and the identification of the haematopoietic cytokine IL-3 as a Zfp36l1 target (Stoecklin et al., 2002).

During mouse embryogenesis, the yolk sac blood islands are the first site of hematopoietic activity. Blood islands contain endothelial cell precursors and the first primitive hematopoietic precursor cells, the latter comprised predominantly of nucleated erythrocytes (Godin and Cumano, 2002). Zfp36l1 also appears to be required for extra-embryonic erythropoiesis, and the paucity of $TER119^+$ erythroid cells within the yolk sac correlates with the reduction in the number of blood cells observed within the blood islands, and within the intra-embryonic circulation. One possibility is that Zfp36l1 normally functions to degrade an mRNA that encodes an inhibitor of erythroid differentiation. Alternatively, the failure in erythropoiesis may be due to the absence of critical growth factors.

The study presented here also provides new insight into how Zfp36l1 regulates VEGF-A expression. It has previously been reported that Zfp36l1 binds to AU-rich sequences within the 3′ UTR of the *Vegf* transcript and that over-expression of Zfp36l1 decreased the activity of a luciferase reporter containing the rat *Vegf* 3′UTR (Ciais et al., 2004). This led to the suggestion that Zfp36l1 may regulate the stability of *Vegf* mRNA, a hypothesis that was not directly tested in the previous study. We found *Vegf* mRNA stability was not altered in *Zfp36l1*-deficient MEF. Instead, we found that more *Vegf* mRNA was associated with polysomes suggesting a role for Zfp36l1 in the translational repression of *Vegf* mRNA. VEGF expression has previously been shown to be regulated at the level of translation initiation by a mechanism involving c-Myc (Mezquita et al., 2005) and eukaryotic translation initiation factor 4E (Kevil et al., 1996; Chung et al., 2002). AREs play a well-documented role in the translational control of gene expression in addition to regulating mRNA stability (Zhang et al., 2002). Translational control of other ARE containing mRNAs has previously been shown to be mediated by RNA binding proteins such as TIA, HuR, and TIAR (Espel, 2005). Recently, TTP (Zfp36) has been shown to become associated with polysomes in lipopolysaccharide-stimulated THP-1 cells (Rigby et al., 2005). While the functional significance of this interaction has not been elucidated, taken together with our results, these data may point towards roles of the TTP family in the co-ordination of mRNA translation and degradation.

Hypoxia markers (such as pimonidazole) have illustrated regions of hypoxia during normal embryonic development (Lee et al., 2001) with development of the vascular systems and placenta influenced by responses to O_2 availability. Establishment of the placental and fetal circulation by E9.0–9.5 permits nutrient and gaseous exchange to the developing embryo. During normal embryonic development, maintenance of a hypoxic environment may tightly regulate VEGF levels to establish normal placental, cardiovascular, and hematopoietic development (Kozak et al., 1997; Maltepe et al., 1997; Iyer et al., 1998; Adelman et al., 2000). Our data now identify *Zfp36l1* as a negative regulator of VEGF production during normal embryonic development. Tightly regulated VEGF levels are also crucial in neovascularisation associated with tumor angiogenesis. It will be interesting to learn if *Zfp36l1* regulates VEGF in this and other settings.

EXPERIMENTAL PROCEDURES

Generation of Mice Carrying a Germline Mutation of Zfp36l1

A 6-kb *Eco*RI fragment encompassing both exons of *Zfp36l1* was isolated from a 129/Sv genomic λ phage library (Stratagene). The positions of the 5′ and 3′ UTRs were assigned using the published mouse cDNA sequence (Varnum et al., 1991) accession number M58566. The *Zfp36l1* gene was disrupted by replacing part of the first zinc finger between *Eco47*III and *Bst*BI (Fig. 1A) with a neomycin cassette derived from pPNT (Tybulewicz et al., 1991). This introduced a new *Bam*HI site into the targeted exon 2. Southern blot analysis with a 450-bp *Eco*RI/*Pst*I fragment external to the targeting vector (probe B), yields a 4.4-kb *Bam*HI fragment from the wild-type allele and a 3.1-kb fragment from the targeted allele. E14 ES cells were transfected, selected, and screened using standard methods. Positive clones were re-screened using a 170-bp *Eco*RI/*Kpn*I fragment (probe A) from a region 5′ of the targeting vector. Probe A yields a 6.2-kb fragment upon digestion of the targeted allele with *Hin*dIII/*Xho*I, whilst the wild-type allele yields an 8-kb fragment (not shown).

Two independently targeted ES cell clones were injected into C57BL/6 blastocysts and male chimeras were mated with B6D2 F1 female mice to generate offspring of a mixed background. Mice were genotyped by Southern blot analysis or by PCR using the following primers: P1 5′-AGAGAGACTGGCCTATCAGATGGAGAGGTG-3′; P2 5′- GGGACTGTCTTGTGTGAAAGGCTCTCTGAG-3′; P3 5′- TAAAGCTATGCTGGAGGCGGGGACGGTCA-3′; to generate a 750-bp product for the wt allele and a 350-bp product for the mutant allele. Genotyping of E9.5 embryo DNA from heterozygous matings was performed by Southern blot analysis or PCR of visceral yolk sac DNA.

RT PCR analysis of total RNA from *Zfp36l1* heterozygous (+/−) and homozygous (−/−) E9.5 embryos was performed using intron-spanning primers to verify the absence of *Zfp36l1* mRNA in null embryos: *Zfp36l*1 forward primer (5′- GACCTTCACACACACCAGAT) located in exon 1, reverse primer (5′- GCTATGCTGGAGGCGGGGA), located 3′ of the second zinc finger in exon 2, to yield a product of 650 bp; *Hprt* primers were used to verify the integrity of the template RNA (*Hprt* forward primer (5′-GTTGGATACAGGCCAGACTTTGTTG), reverse primer (5′-GAGGGTAGGCTGGCCTATAGGCT), to yield a product of 350 bp).

Transgenic mice expressing a *lacZ* reporter under the control of an *SCL* promoter and 3′ enhancer (line 2269; Sanchez et al., 1999) were obtained

from A. R. Green (University of Cambridge). These mice exhibit *lacZ* expression specifically in blood vessels and hematopoietic tissue. *SCL lacZ* transgenic mice were bred with *Zfp36l1* heterozygous mice to derive *SCL lacZ* transgenic embryos.

Mice were bred and maintained at the Babraham Institute Small Animal Barrier Unit according to UK Home Office guidelines.

Analysis of Embryos

Embryos were harvested from timed matings between 8.5 and 13.5 days gestation (with day 0.5 defined as the morning of the day of detecting a vaginal plug). Embryos were dissected and photographed using a Leitz MZ75 dissecting microscope. Images were captured using a Leica DC100 digital camera using the Leica DC Viewer program.

At E9.5, VEGF levels in whole embryo extracts were determined as described (Miquerol et al., 2000), normalising for total protein content. Optical projection tomography of X-gal stained *SCL lacZ* transgenic embryos was performed as a service by Bioptonics, MRC Technology, Edinburgh, UK (www.bioptonics.com). X-gal staining of *SCL lacZ* transgenic embryos was performed as previously described (Sanchez et al., 2001). Dissected yolk sac tissue was mounted under coverslips to view at a higher magnification under phase contrast illumination.

Flow Cytometric Analysis of Yolk Sac Cells

Individual yolk sacs were removed from E9.5 embryos. Cells were isolated from individual yolk sacs and flow cytometric analysis was performed as described previously (Sanchez et al., 2001).

Immunohistochemistry

Embryos were dissected at E8.5–9.5, keeping the visceral yolk sac intact, and a small incision was made to remove the head in order to extract DNA for genotyping. Whole mount staining of embryos and yolk sacs with anti-PECAM-1 antibody (MEC13.3, BD BioSciences, UK) was performed as described previously (Schlaeger et al., 1995). For histological analysis, freshly dissected embryos were fixed in 4% paraformaldehyde for 2 hr at room temperature before dehydration through ethanol, then were paraffin-embedded for sectioning following standard protocols. Sections were stained with hematoxylin and eosin (H & E) using standard methods.

Polyclonal antibodies to label cytokeratin (Z0622) of trophoblast cells and von Willebrand factor (A0082) of endothelial cells were from DAKOCytomation, UK (Adamson et al., 2002). Sections were dewaxed, rehydrated, and pre-treated with 0.02 mg/ml proteinase K (Sigma) for cytokeratin staining, or pre-treated with 1 mg/ml trypsin (Sigma) for von Willebrand factor staining. Sections were blocked in 2% goat serum/2% BSA, incubated with the primary antibodies, followed by incubation with biotinylated goat anti-rabbit IgG and Vectastain Elite ABC kit (both from Vector Laboratories, UK), then developed using DAB as the substrate. Slides were counterstained with hematoxylin and mounted in DPX. Images were captured digitally using a Zeiss Axiophot microscope and high-resolution Spot Diagnostic digital camera and assembled using Adobe Photoshop® v 7.0. To examine cardiac structure, E9.5 embryos were fixed in 4% glutaraldehyde in 0.1 M PIPES buffer for 6 hr, rinsed in buffer and treated with 1% osmium tetroxide for 2 hr, rinsed in deionised water and dehydrated in an ascending series of ethanol, and rinsed twice in acetonitrile and embedded in Spurr's epoxy resin. Two-micrometer sections were cut with a Leica Ultracut UCT and stained with methylene blue.

In Situ Hybridisation

In situ hybridisation was performed by Phylogeny, Ohio, USA (www.phylogenyinc.com) using [^{35}S]-UTP-labelled cRNA transcripts following standard protocols. Slides were lightly counterstained with toluidine blue and analysed using light- and dark-field optics of a Zeiss Axiophot microscope. The probe was nucleotides 1,116–1,468 of *Zfp36l1* GenBank accession number M58566.

Establishment and Analysis of Fibroblast Lines

Individual embryos at E9.5 were mechanically disrupted and cultured in 96-well plates in Dulbecco's modified Eagle's medium containing 15% FCS, 2 mM glutamine for 5 days to derive independent embryonic fibroblast (MEF) lines. MEF at p1 were immortalised using retrovirus containing SV40 T antigen (Jat and Sharp, 1989). For measurement of VEGF levels, 1.25×10^5 MEF from individual embryos were plated in individual wells of a 6-well plate in DMEM medium containing 10% FCS, 2 mM glutamine, and cultured under normoxic (21% O_2) or hypoxic (1% O_2) conditions for 24 hr. VEGF in the supernatants was measured by ELISA (R&D Systems, UK) following the manufacturer's protocol. Remaining cells were either lysed immediately in SDS-PAGE sample buffer, or removed using trypsin treatment, washed in PBS and RNA prepared using an RNeasy miniprep kit (Qiagen, UK). Cell lysates were analysed by 10% SDS-PAGE and transferred to PVDF membranes. Western blot analysis was performed by standard methods using horseradish peroxidase-conjugated secondary antibodies (DAKOCytomation) and enhanced chemiluminescence reagents (Amersham Biosciences, UK). The glucose transporter 1 (Glut-1) antibody was from Chemicon International (Temecula, CA). An antibody directed against the C-terminus of Zfp36l1 was generated in our laboratory (S.E.B. and M.T., unpublished data).

Northern and Dot Blot Analysis

Northern and dot blot analysis of RNA were performed using standard protocols. The mouse *Vegf* probe was a gift from K. Luukko (University of Bergen, Norway). The hybridisation signal was quantified using a Fuji FLA3000 Imager. Northern blots were stripped and re-hybridised using a probe for γ-actin to normalise for RNA loading. For the measurement of mRNA half life, mutant (−/−) and wild-type (+/+) MEF were treated with 100 μM cobalt chloride for 4 hr, followed by actinomycin D treatment (5 μg/ml). MEF were harvested at the

indicated time points and total mRNA extracted. *Vegf-a* RNA levels were measured by quantitative PCR or Northern blot analysis.

Real Time PCR Analysis

Reverse transcription (RT) PCR analysis was performed on total RNA prepared from wild-type (+/+) and mutant (−/−) MEF. RNA was subjected to cDNA first-strand synthesis using a high-capacity cDNA archive kit (Applied Biosystems). Quantitative PCR analysis was performed using FAM-labelled probe sets from Applied Biosystems, according to the manufacturer's protocol using an ABI Prism 7700 real-time PCR detection system. Comparative Ct values were used to calculate the quantity of *Vegf-a* RNA relative to *hprt*.

Polysome Analysis

MEF were serum starved overnight, then incubated in complete medium for 3 hr. Cells were washed with cold PBS containing 100 μg/ml cycloheximide, removed using trypsin, pelleted by centrifugation, and resuspended in hypotonic lysis buffer (10 mM KCl, 10 mM Tris, pH 7.2, 10 mM $MgCl_2$, 20 mM dithiothreitol, 100 μg/ml cycloheximide, 0.5 mg/ml heparin, 0.5% NP-40, and 100U/ml RNaseout; Invitrogen) for 10 min on ice before disruption by homogenisation. Nuclei were removed by centrifugation 10,000*g* 10 min at 4°C and the cytoplasmic extracts layered onto a 15–40% sucrose gradient and centrifuged at 4°C for 120 min at 38,000rpm in a SW41Ti rotor. Fractions were collected from the top of the gradient and absorbance of each fraction measured at 254 nm. SDS was added to 1% and fractions stored at −80°C. Following proteinase K digestion, total RNA from each fraction was prepared by phenol-chloroform extraction and isopropanol precipitation, then dot-blotted onto Hybond XL membrane (Amersham Biosciences) and hybridised using standard protocols with a probe against m*Vegf*. The hybridisation signal was normalised to the amount of RNA blotted.

Statistical Analyses

Statistical analyses were performed using a Student's unpaired *t*-test. Values for $P < 0.05$ were considered significant.

ACKNOWLEDGMENTS

We thank lab members for advice and assistance and the staff of the Babraham Institute Small Animal Barrier Unit; Jeremy Skepper for expert advice and sectioning of epoxy-embedded embryos; Tony Green for advice and SCL-LacZ mice; and Andrew McKenzie, Myriam Hemberger, and Elena Vigorito for comments on the manuscript. M.J.S. was funded by an MRC Career Development Award and by the Ministerio de Educacion y Ciencia grant number SAF2003-07214. M.T. is an MRC Senior Fellow. Frozen embryos from line 2 have been deposited at FESA, MRC Harwell, Oxford, UK (http://www.mgu.har.mrc.ac.uk/fesa/fesa.html).

REFERENCES

Adams RH, Porras A, Alonso G, Jones M, Vintersten K, Panelli S, Valladares A, Perez L, Klein R, Nebreda AR. 2000. Essential role of p38α MAP kinase in placental but not embryonic cardiovascular development. Mol Cell 6:109–116.

Adamson SL, Lu Y, Whiteley KJ, Holmyard D, Hemberger M, Pfarrer C, Cross JC. 2002. Interactions between trophoblast cells and the maternal and fetal circulation in the mouse placenta. Dev Biol 250:358–373.

Adelman DM, Gertsenstein M, Nagy A, Simon MC, Maltepe E. 2000. Placental cell fates are regulated in vivo by HIF-mediated hypoxia responses. Genes Dev 14: 3191–3203.

Bakheet T, Frevel M, Williams BR, Greer W, Khabar KS. 2001. ARED: human AU-rich element-containing mRNA database reveals an unexpectedly diverse functional repertoire of encoded proteins. Nucleic Acids Res 29:246–254.

Barak Y, Nelson MC, Ong ES, Jones YZ, Ruiz-Lozano P, Chien KR, Koder A, Evans RM. 1999. PPAR gamma is required for placental, cardiac, and adipose tissue development. Mol Cell 4:585–595.

Barnard RC, Pascall JC, Brown KD, McKay IA, Williams NS, Bustin SA. 1993. Coding sequence of ERF-1, the human homologue of Tis11b/cMG1, members of the Tis11 family of early response genes. Nucleic Acids Res 21:3580.

Bustin SA, Nie XF, Barnard RC, Kumar V, Pascall JC, Brown KD, Leigh IM, Williams NS, McKay IA. 1994. Cloning and characterization of ERF-1, a human member of the Tis11 family of early-response genes. DNA Cell Biol 13:449–459.

Carballo E, Gilkeson GS, Blackshear PJ. 1997. Bone marrow transplantation reproduces the tristetraprolin-deficiency syndrome in recombination activating gene-2 (−/−) mice. Evidence that monocyte/macrophage progenitors may be responsible for TNFalpha overproduction. J Clin Invest 100:986–995.

Carmeliet P, Ferreira V, Breier G, Pollefeyt S, Kieckens L, Gertsenstein M, Fahrig M, Vandenhoeck A, Harpal K, Eberhardt C, Declercq C, Pawling J, Moons L, Collen D, Risau W, Nagy A. 1996. Abnormal blood vessel development and lethality in embryos lacking a single VEGF allele. Nature 380:435–439.

Chung J, Bachelder RE, Lipscomb EA, Shaw LM, Mercurio AM. 2002. Integrin (alpha 6 beta 4) regulation of eIF-4E activity and VEGF translation: a survival mechanism for carcinoma cells. J Cell Biol 158:165–174.

Ciais D, Cherradi N, Bailly S, Grenier E, Berra E, Pouyssegur J, Lamarre J, Feige JJ. 2004. Destabilization of vascular endothelial growth factor mRNA by the zinc-finger protein TIS11b. Oncogene 23: 8673–8680.

Damert A, Miquerol L, Gertsenstein M, Risau W, Nagy A. 2002. Insufficient VEGFA activity in yolk sac endoderm compromises haematopoietic and endothelial differentiation. Development 129: 1881–1892.

Drake CJ, Little CD. 1995. Exogenous vascular endothelial growth factor induces malformed and hyperfused vessels during embryonic neovascularization. Proc Natl Acad Sci USA 92:7657–7661.

DuBois RN, McLane MW, Ryder K, Lau LF, Nathans D. 1990. A growth factor-inducible nuclear protein with a novel cysteine/histidine repetitive sequence. J Biol Chem 265:19185–19191.

Espel E. 2005. The role of the AU-rich elements of mRNAs in controlling translation. Semin Cell Dev Biol 16:59–67.

Ferrara N, Davis-Smyth T. 1997. The biology of vascular endothelial growth factor. Endocr Rev 18:4–25.

Ferrara N, Carver-Moore K, Chen H, Dowd M, Lu L, O'Shea KS, Powell-Braxton L, Hillan KJ, Moore MW. 1996. Heterozygous embryonic lethality induced by targeted inactivation of the VEGF gene. Nature 380:439–442.

Fong GH, Rossant J, Gertsenstein M, Breitman ML. 1995. Role of the Flt-1 receptor tyrosine kinase in regulating the assembly of vascular endothelium. Nature 376:66–70.

Godin I, Cumano A. 2002. The hare and the tortoise: an embryonic haematopoietic race. Nat Rev Immunol 2:593–604.

Gomperts M, Pascall JC, Brown KD. 1990. The nucleotide sequence of a cDNA encoding an EGF-inducible gene indicates the existence of a new family of mitogen-induced genes. Oncogene 5:1081–1083.

Hemberger M, Cross JC. 2001. Genes governing placental development. Trends Endocrinol Metab 12:162–168.

Heximer SP, Forsdyke DR. 1993. A human putative lymphocyte G0/G1 switch gene homologous to a rodent gene encoding a zinc-binding potential transcription factor. DNA Cell Biol 12:73–88.

Hiratsuka S, Minowa O, Kuno J, Noda T, Shibuya M. 1998. Flt-1 lacking the tyrosine kinase domain is sufficient for normal development and angiogenesis in mice. Proc Natl Acad Sci USA 95:9349–9354.

Iyer NV, Kotch LE, Agani F, Leung SW, Laughner E, Wenger RH, Gassmann M, Gearhart JD, Lawler AM, Yu AY, Semenza GL. 1998. Cellular and developmental control of O2 homeostasis by hypoxia-inducible factor 1 alpha. Genes Dev 12:149–162.

Jat PS, Sharp PA. 1989. Cell lines established by a temperature-sensitive simian virus 40 large-T-antigen gene are growth restricted at the nonpermissive temperature. Mol Cell Biol 9:1672–1681.

Kearney JB, Kappas NC, Ellerstrom C, DiPaola FW, Bautch VL. 2004. The VEGF receptor flt-1 (VEGFR-1) is a positive modulator of vascular sprout formation and branching morphogenesis. Blood 103:4527–4535.

Kevil CG, De Benedetti A, Payne DK, Coe LL, Laroux FS, Alexander JS. 1996. Translational regulation of vascular permeability factor by eukaryotic initiation factor 4E: implications for tumor angiogenesis. Int J Cancer 65:785–790.

Kozak KR, Abbott B, Hankinson O. 1997. ARNT-deficient mice and placental differentiation. Dev Biol 191:297–305.

Lai WS, Stumpo DJ, Blackshear PJ. 1990. Rapid insulin-stimulated accumulation of an mRNA encoding a proline-rich protein. J Biol Chem 265:16556–16563.

Lai WS, Carballo E, Strum JR, Kennington EA, Phillips RS, Blackshear PJ. 1999. Evidence that tristetraprolin binds to AU-rich elements and promotes the deadenylation and destabilization of tumor necrosis factor alpha mRNA. Mol Cell Biol 19:4311–4323.

Lai WS, Carballo E, Thorn JM, Kennington EA, Blackshear PJ. 2000. Interactions of CCCH zinc finger proteins with mRNA. Binding of tristetraprolin-related zinc finger proteins to AU-rich elements and destabilization of mRNA. J Biol Chem 275:17827–17837.

Lee YM, Jeong CH, Koo SY, Son MJ, Song HS, Bae SK, Raleigh JA, Chung HY, Yoo MA, Kim KW. 2001. Determination of hypoxic region by hypoxia marker in developing mouse embryos in vivo: a possible signal for vessel development. Dev Dyn 220:175–186.

Levy AP, Levy NS, Wegner S, Goldberg MA. 1995. Transcriptional regulation of the rat vascular endothelial growth factor gene by hypoxia. J Biol Chem 270:13333–13340.

Ma Q, Herschman HR. 1991. A corrected sequence for the predicted protein from the mitogen-inducible TIS11 primary response gene. Oncogene 6:1277–1278.

Maclean KN, See CG, McKay IA, Bustin SA. 1995. The human immediate early gene BRF1 maps to chromosome 14q22–q24. Genomics 30:89–90.

Maltepe E, Schmidt JV, Baunoch D, Bradfield CA, Simon MC. 1997. Abnormal angiogenesis and responses to glucose and oxygen deprivation in mice lacking the protein ARNT. Nature 386:403–407.

Mezquita P, Parghi SS, Brandvold KA, Ruddell A. 2005. Myc regulates VEGF production in B cells by stimulating initiation of VEGF mRNA translation. Oncogene 24:889–901.

Miquerol L, Langille BL, Nagy A. 2000. Embryonic development is disrupted by modest increases in vascular endothelial growth factor gene expression. Development 127:3941–3946.

Ning ZQ, Norton JD, Li J, Murphy JJ. 1996. Distinct mechanisms for rescue from apoptosis in Ramos human B cells by signaling through CD40 and interleukin-4 receptor: role for inhibition of an early response gene, Berg36. Eur J Immunol 26:2356–2563.

Ramos SB, Stumpo DJ, Kennington EA, Phillips RS, Bock CB, Ribeiro-Neto F, Blackshear PJ. 2004. The CCCH tandem zinc-finger protein Zfp36l2 is crucial for female fertility and early embryonic development. Development 131:4883–4893.

Rigby WF, Roy K, Collins J, Rigby S, Connolly JE, Bloch DB, Brooks SA. 2005. Structure/function analysis of tristetraprolin (TTP): p38 stress-activated protein kinase and lipopolysaccharide stimulation do not alter TTP function. J Immunol 174:7883–7893.

Rossant J, Cross JC. 2001. Placental development: lessons from mouse mutants. Nat. Rev Genet 2:538–548.

Sanchez M, Gottgens B, Sinclair AM, Stanley M, Begley CG, Hunter S, Green AR. 1999. An SCL 3′ enhancer targets developing endothelium together with embryonic and adult haematopoietic progenitors. Development 126:3891–3904.

Sanchez MJ, Bockamp EO, Miller J, Gambardella L, Green AR. 2001. Selective rescue of early haematopoietic progenitors in Scl(−/ −) mice by expressing Scl under the control of a stem cell enhancer. Development 128:4815–4827.

Schlaeger TM, Qin Y, Fujiwara Y, Magram J, Sato TN. 1995. Vascular endothelial cell lineage-specific promoter in transgenic mice. Development 121:1089–1098.

Sharpe J, Ahlgren U, Perry P, Hill B, Ross A, Hecksher-Sorensen J, Baldock R, Davidson D. 2002. Optical projection tomography as a tool for 3D microscopy and gene expression studies. Science 296:541–545.

Stoecklin G, Colombi M, Raineri I, Leuenberger S, Mallaun M, Schmidlin M, Gross B, Lu M, Kitamura T, Moroni C. 2002. Functional cloning of BRF1, a regulator of ARE-dependent mRNA turnover. EMBO J 21:4709–4718.

Stumpo DJ, Byrd NA, Phillips RS, Ghosh S, Maronpot RR, Castranio T, Meyers EN, Mishina Y, Blackshear PJ. 2004. Chorioallantoic fusion defects and embryonic lethality resulting from disruption of Zfp36L1, a gene encoding a CCCH tandem zinc finger protein of the Tristetraprolin family. Mol Cell Biol 24:6445–6455.

Taylor GA, Carballo E, Lee DM, Lai WS, Thompson MJ, Patel DD, Schenkman DI, Gilkeson GS, Broxmeyer HE, Haynes BF, Blackshear PJ. 1996. A pathogenetic role for TNF alpha in the syndrome of cachexia, arthritis, and autoimmunity resulting from tristetraprolin (TTP) deficiency. Immunity 4:445–454.

Tybulewicz VL, Crawford CE, Jackson PK, Bronson RT, Mulligan RC. 1991. Neonatal lethality and lymphopenia in mice with a homozygous disruption of the c-abl proto-oncogene. Cell 65:1153–1163.

Varnum BC, Lim RW, Sukhatme VP, Herschman HR. 1989. Nucleotide sequence of a cDNA encoding TIS11, a message induced in Swiss 3T3 cells by the tumor promoter tetradecanoyl phorbol acetate. Oncogene 4:119–120.

Varnum BC, Ma QF, Chi TH, Fletcher B, Herschman HR. 1991. The TIS11 primary response gene is a member of a gene family that encodes proteins with a highly conserved sequence containing an unusual Cys-His repeat. Mol Cell Biol 11:1754–1758.

Ylikorkala A, Rossi DJ, Korsisaari N, Luukko K, Alitalo K, Henkemeyer M, Makela TP. 2001. Vascular abnormalities and deregulation of VEGF in Lkb1-deficient mice. Science 293:1323–1326.

Zhang T, Kruys V, Huez G, Gueydan C. 2002. AU-rich element-mediated translational control: complexity and multiple activities of trans-activating factors. Biochem Soc Trans 30:952–958.